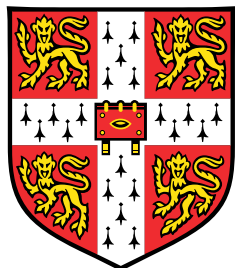


# **Long-term impacts of fire on forest carbon in the Sierra Nevada mountains**



**Jovana Knezevic**

Supervisor: Dr. David Coomes

Dr. Adam Pellegrini

AI4ER CDT  
University of Cambridge

This thesis is submitted for the degree of  
*Master of Research in Environmental Data Science*

June 2023



## **Declaration**

This report is the result of my own work and includes nothing which is the outcome of work done in collaboration, except where specifically indicated in the text and/or bibliography.

Jovana Knezevic  
June 2023



## Abstract

Assessment of post-fire vegetation loss and recovery is instrumental for comprehensive carbon accounting and estimation of forest carbon permanence, necessary for effective implementation of nature-based solutions. We combine space-for-time substitution with synthetic counterfactuals to estimate post-fire carbon sequestration in the Sierra Nevada forests, using aboveground biomass density (AGBD) estimates derived from GEDI, a spaceborne lidar launched in 2018. To overcome the challenge of extrapolating multi-decadal recovery trends from only a few years of recent data, we employ space-for-time substitution - a widely used technique that requires careful application to avoid erroneous results. We show that space-for-time analysis works best in combination with controls to evaluate relative, rather than absolute, recovery. We demonstrate this by applying it to NDVI for which we have long-term time series data, and then transferring the methodology to analyze carbon recovery. To find a suitable control for biomass recovery, we evaluate numerous algorithms through placebo on unburned areas. Our results show that commonly used controls perform poorly on these tests ( $R^2 < 0.2$ ) We find that using ML to predict synthetic biomass counterfactuals from historical spectral data yields the highest accuracy ( $R^2 = 0.57$ ). Using our new methodology, we compare NDVI and AGBD recovery trends, and show that while foliage fully recovers within 25 years, biomass recovery lags behind. After 35 years of recovery, wildfire effects on stored carbon still persist. Our study highlights the limitations of using optical data alone as a proxy for carbon sequestration, but emphasizes its value in creating improved biomass counterfactuals. We note that GEDI may have limited ability to track initial recovery in areas with low or medium severity burns but exhibits greater sensitivity to biomass accumulation in high severity burn areas. In conclusion, our results support the integration of space-for-time substitution with counterfactuals to monitor carbon sequestration after forest disturbances. This approach contributes towards more accurate long-term carbon accounting for nature-based solutions and post-fire recovery management.

Word count = 4998

# Table of contents

<b>1</b>	<b>Introduction</b>	<b>1</b>
<b>2</b>	<b>Data</b>	<b>5</b>
2.1	Study Area . . . . .	5
2.2	GEDI . . . . .	5
2.3	Raster Datasets . . . . .	7
2.3.1	Landsat . . . . .	7
2.3.2	Terrain and soil . . . . .	8
2.3.3	Land cover . . . . .	8
2.3.4	Historic Fire Record and Mapping of Burn Severity . . . . .	8
<b>3</b>	<b>Analysis Methods</b>	<b>11</b>
3.1	Data fusing and filtering . . . . .	11
3.2	Reconstruction of post-fire recovery trajectories . . . . .	12
3.2.1	Space-for-time substitution . . . . .	12
3.2.2	NDVI recovery reconstruction . . . . .	12
3.3	Burn area counterfactuals of biomass . . . . .	12
3.3.1	Using unburned areas as placebos for validation of controls . . . . .	13
3.4	Using Random Forests to Predict Aboveground Biomass from Landsat and Terrain Data . . . . .	14
3.4.1	Selecting calibration data . . . . .	14
3.4.2	Random forest training . . . . .	15
3.4.3	Random forest inference . . . . .	15
3.5	Code and data availability . . . . .	16
<b>4</b>	<b>Results</b>	<b>17</b>
4.1	Validation of space-for-time substitution using NDVI historic data . . . . .	17
4.2	Evaluation of controls on unburned areas . . . . .	18

4.3 Post-fire NDVI and AGBD recovery . . . . .	19
4.3.1 NDVI recovery using time series analysis . . . . .	19
4.3.2 Aboveground biomass recovery using space-for-time analysis . . .	20
4.3.3 Effects of severity on vegetation recovery . . . . .	21
<b>5 Discussion</b>	<b>25</b>
5.1 Post-fire Recovery . . . . .	25
5.2 Space-for-time Substitution with Counterfactuals . . . . .	26
5.3 Limitations . . . . .	26
<b>References</b>	<b>27</b>
<b>Appendix A Supplementary Information</b>	<b>33</b>
A.1 Limitations of optical data . . . . .	33
A.2 GEDI detects statistically significant carbon losses in areas of medium and high burn severity, but not in low burn severity . . . . .	34
A.3 Supplementary Figures . . . . .	37
A.3.1 Validation of space-for-time substitution using NDVI historic data .	37
A.3.2 NDVI Recovery . . . . .	37
A.3.3 GEDI geolocation error . . . . .	37

# Chapter 1

## Introduction

Nature-based solutions (NbS) play a critical role in climate change mitigation through natural carbon sequestration [44], but face implementation challenges due to impermanence of forest carbon [11, 10]. Wildfire is a leading permanence risk for forest-stored carbon [9, 10]. In the western United States, it is estimated that climate change has doubled the extent of forest fire area over the past 30 years [8], and that fire frequency and size have increased [23]. As small shifts in fire regimes can substantially affect forest capacity to sequester carbon [41], it is important to quantify post-fire vegetation loss (carbon source) and recovery (carbon sink). Assessing the ability to return to pre-fire state is important for implementation of restoration efforts, monitoring of ecosystem health and comprehensive carbon accounting necessary for effective NbS implementation [28, 45, 45].

Due to its multi-decadal historical record, most studies of post-fire recovery analyse data from optical sensors to estimate vegetation response. Most frequently the Normalized Difference Vegetative Index (NDVI) is used to assess change [33, 45, 18, 30, 47]. However, NDVI is known to saturate for denser canopies; while useful for studying short-term recovery, it provides limited insights into long-term recovery as vegetation grows past the saturation limit [14, 48]. In addition to optical sensors, lidars have been used to describe post-fire vegetation structure and detect successional stages, but obtaining lidar data at regional level has been cost prohibitive [17]. Global Ecosystem Dynamics Investigation (GEDI) is a recently launched space-born lidar sampler designed to measure forest structure and estimate carbon stocks [16]. GEDI provides estimates of aboveground biomass density (AGBD) for millions of 25 meter wide LiDAR shots. Recent studies have used GEDI to estimate post-disturbance recovery [22], but few have used it to look at recovery following a fire [32, 24], and none to our knowledge have looked at post-fire recovery of GEDI's carbon metrics.

GEDI has two main limitations: it's spatially sparse, lacking wall-to-wall coverage, and temporally limited, being launched in 2018 and providing only three years of data [16, 43]. This represents a challenge when attempting to look at multi-decadal post-fire recovery. Recent studies have tried to fuse Landsat and GEDI datasets, attempting to provide the best of both worlds: spatial and temporal coverage from Landsat, with structural metrics of GEDI [40, 31, 43]. The results of these studies indicate that while the reconstruction of structural metrics is not perfect, models can exploit the existing correlations between Landsat reflectances and metrics like canopy height, especially when calibrated to local areas or forest types [20].

Space-for-time substitution, a widely used methodology for dealing with the lack of historic data, may be more effective when used to reconstruct relative, rather than absolute, temporal trends. Relative recovery is commonly calculated as a measurement of interest relative to its pre-fire value [21], a representative value for the ecosystem [42], or a counterfactual representing the measurement if the forest had not burned [45]. Unburned regions around the fire perimeter have often been used as controls, assuming spatial auto-correlation between nearby forests[24]. However, these controls may be inadequate, and synthetic controls have shown better outcomes [45]. The use of counterfactuals as controls has been extensively employed in estimating carbon additionality for nature-based carbon credits. These studies have highlighted that the choice of counterfactual can significantly influence the final result, emphasizing the importance of evaluating control quality [49]. While many studies of post-fire recovery use controls, most do not quantitatively justify their choice of controls. Similarly, studies use space-for-time to construct both relative and absolute recovery chronosequences, but it isn't clear which approach yields higher reconstruction accuracy.

In this project, we develop and evaluate a framework for reconstructing carbon recovery trajectories using space-for-time substitution. We assess the rate of relative recovery by analyzing the ratio between GEDI aboveground biomass density (AGBD) measurements and synthetic controls. The main objectives of our study can be summarized as follows:

1. Evaluate effectiveness of space-for-time substitution in reconstruction of relative and absolute long-term recovery trajectories.
2. Develop a framework for evaluating controls on unburned regions as placebos, and measure the accuracy of previously proposed counterfactual-finding algorithms.

3. Use machine learning to create controls that outperform random sampling of nearby areas.
4. Use our methodology to conduct a comparative analysis of post-fire aboveground biomass and NDVI loss and recovery in Sierra Nevada mountains.

While in this study we focus on AGBD recovery, it is directly related to carbon stock recovery. By multiplying AGBD by 0.51 (conversion factor for coniferous forests) we can obtain aboveground carbon density (ACD) [25].



# **Chapter 2**

## **Data**

### **2.1 Study Area**

The study area encompasses the Sierra Nevada conservancy area and its surrounding regions, with a total surface area of 145,646 km<sup>2</sup> (Figure 2.1). This region experiences Mediterranean climate, with dry summers and moist winters [27]. The Sierra Nevada exhibits significant topographic variation, experiencing steep slopes with elevation ranging from 149m to 4421m. Vegetation varies with elevation, with lower elevations primarily dominated by chaparral shrubs (380m to 1500m), mixed conifer forests occurring at mid-elevations ( 600 to 2500m, depending on latitude), and fir forest and subalpine forests residing at higher elevations ( 1700m to 2900m) [27]. Forested areas often display a fragmented pattern, interspersed with meadows or patches of chaparral [27]. The study primarily focuses on areas classified as "forest" by the land cover classifier, without further stratification based on species composition.

### **2.2 GEDI**

GEDI is a full waveform, space-born lidar. It launched in 2018 with the purpose of measuring vegetation vertical structure and estimating aboveground biomass density in temperate and tropical forests between 51.6° to -51.6° latitude. GEDI instrument operates 3 lasers with 8 beam ground transects, spaced 600m apart. Each GEDI sample is called a footprint with a spatial resolution of 25 meters in diameter, and geolocation error of 10m [16]. In this project, we used the GEDI product Level 4A.

GEDI Level 4A product provides estimations of Above Ground Biomass Density (AGBD) measured in Mg/ha. AGBD is derived from the Level 2A product, which captures relative

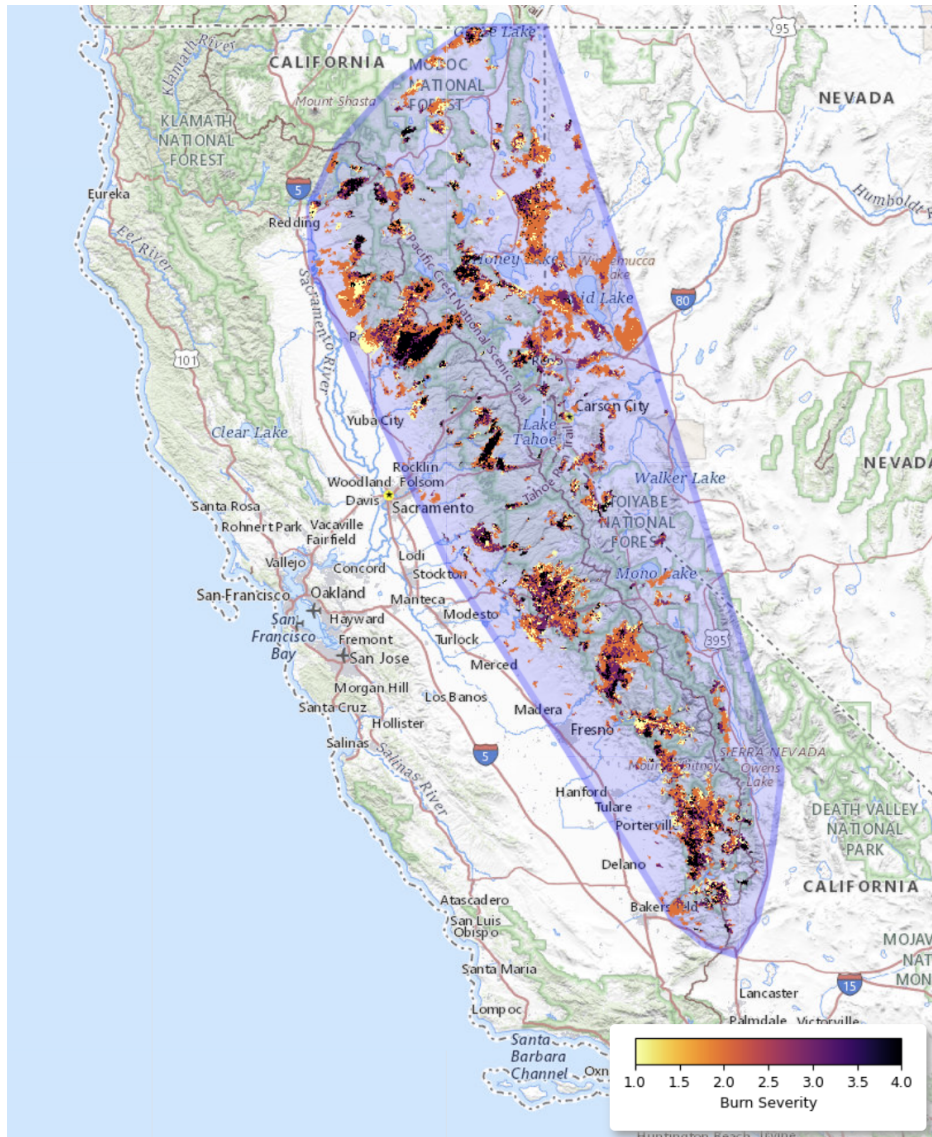


**Fig. 2.1** – A map showing the study area shaded in blue. It covers the entire Sierra Nevada mountain range. Overlaid on top are the areas that burned in the period of 1984 to 2022, colored based on their burn severity.

canopy heights (RH). Level 4A employs Ordinary Least Square (OLS) parametric models to estimate AGBD from a range of height metrics, and calibrates the models on pairs of geographical regions and plant functional types (PFTs) [29]. According to the product's geographical and plant strata, Sierra Nevada mountain range predominantly falls into the category of North America's evergreen needleleaf trees (ENT) [29]. Consequently, AGBD values for this region are determined using two specific height metrics: RH70 and RH98, which indicate the heights at which the 70th and 98th quantiles of returned energy are reached relative to the ground [29]. As a result, the changes in GEDI's aboveground biomass

**Table 2.1** – Parameters and criteria used to do initial filtering of GEDI shots

Parameter	Criteria
Level 2 Quality Flag	= 1
Level 4 Quality Flag	= 1
Degrade Flag	= 0
Beam Sensitivity	> 0.9

estimates will correspond to the changes in the mid and upper levels of the canopy, and not the understory.

We acquired GEDI samples from the period of April 2019 until December 2022. All GEDI footprints were filtered to meet the quality criteria utilized in other GEDI recovery studies [34] [22], described in the Table 2.1. They were further selected according to the historic burn record, which is discussed in Chapter 3. After the initial quality filtering, 9,884,257 shots remained for further analysis.

## 2.3 Raster Datasets

### 2.3.1 Landsat

Landsat provides benefits of global wall-to-wall coverage and extensive historical record of optical spectral bands at 30m resolution. We obtained annual mean composite images spanning from 1984 to 2022 from the Google Earth Engine Surface Reflectance Collection 2 [1]. The Landsat program encompasses multiple satellite missions, each operating during distinct time periods. We utilized data from Landsat 5 (1984-1999), Landsat 7 (1999-2013), and Landsat 8 (2013-2022). Landsat 5 and 7 have lower spectral resolution than Landsat 8. To ensure data comparability across time, we selected Tier 1 datasets, which have undergone inter-calibration across different sensors and have been recommended by USGS for time-series analysis [2]. Annual composites were created according to the algorithm suggested by Parks ([36]), including radiometric normalization and cloud masking. We used their code available at <https://code.earthengine.google.com/c76157be827be2f24570df50cca427e9> as the starting point.

We used Landsat data in several of our analyses, which will be outlined in the proceeding sections in more detail. We collected the data from all optical bands (SR1 - SR7), and calculated NDVI. NDVI estimates vegetation greenness, and is calculated as a normalized ratio between red and near infrared values using the formula:

$$NDVI = \frac{NIR - Red}{NIR + Red} \quad (2.1)$$

Note that Landsat 5 and 7 have different band spans than Landsat 8, and the NDVI calculation needed to be adjusted for each satellite [3].

### 2.3.2 Terrain and soil

For the description of terrain, we used NASA's Shuttle Radar Topography Mission (SRTM) Digital Elevation Data at 30m resolution [4]. We derived elevation, aspect and slope as variables of interest. Soil classification at 90m resolution was obtained from US Lithology dataset, that divides soil types into 21 categories [6].

### 2.3.3 Land cover

For land cover classification, we used USFS Landscape Change Monitoring System v2021.7 (LCMS) because of its compatible resolution of 30m, availability dating back to 1985, and ease of access through Google Earth Engine [7]. We used LCMS land cover product that uses Landsat and Sentinel reflectance data as input to a random forest to classify each pixel into 14 land cover classes for each year. In our study we only look at pixels that were categorized as "Trees" one year before fire.

### 2.3.4 Historic Fire Record and Mapping of Burn Severity

Monitoring Trends in Burn Severity (MTBS; <http://www.mtbs.gov/>) dataset provides historic fire records for the United States and fires larger than 1000 acres, in the period of 1984 to 2022, through two products:

- MTBS Burned Area Boundaries dataset was downloaded directly from <https://www.mtbs.gov/direct-download> website. It includes shape files representing geographical perimeters of each fire, with the date of ignition and total area burned. We downloaded fire perimeters for fires that burned between 1984 and 2022.
- MTBS Burn Severity Images were obtained from Google Earth Engine. They represent annual 30m resolution rasters of burned pixels, labeled with burn severity category: low, medium or high. We combined 38 MTBS burn severity images, one for each year in 1984-2022 range, and for each pixel calculated a) the year of its last fire b) the severity category of its last fire.

MTBS uses Landsat-derived delta Normalized Burned Ratio (dNBR) and relative delta Normalized Burned Ratio (rdNBR) indices combined with fire expert's input to determine per-fire thresholds for the classification of burn severity categories [38]. Burn severity is defined as the impact of fire on an ecosystem, and is often categorized as low, medium or high. As an example, stand-replacing fire should be classified as high severity, while surface fire that does not reach the canopy would commonly be classified as low severity [35].



# Chapter 3

## Analysis Methods

### 3.1 Data fusing and filtering

The GEDI data consists of individual footprints with a diameter of 25 meters, sampled along the orbital track of the International Space Station. On the other hand, our remaining data exists in the form of discrete, high-resolution (30m x 30m) images, with wall-to-wall regional coverage. To combine these datasets, we extract values from the images based on the geographic locations of the GEDI shots. In order to minimize the impact of GEDI's geolocation error of 10 meters, we matched each GEDI shot with the surrounding 2x2 or 3x3 image pixels. To ensure avoid sampling from areas with heterogeneous characteristics, we required all neighbouring pixels to have matching values. GEDI shots were then filtered based on the matching image data, and divided into two groups - burned and unburned:

- Unburned include shots that didn't burn since 1984. We require 9 pixels in the 3x3 window (90m x 90m) surrounding the shot to have a burn count of zero.
- Burned include shots in which every surrounding pixel burned only once, in the same year, with the same severity, effectively removing shots from the burn boundaries. For each burned shot we calculated the time difference between the fire year and GEDI sampling year. This is the time that passed since the fire, and represents forest "Recovery time"; it is labeled as such on all the figures. Finally we only look at shots that fell within forests, as defined by  $pft\_class = 1$  flag.

At the end of the filtering, we had 7,829,875 unburned and 417,824 of burned shots.

## 3.2 Reconstruction of post-fire recovery trajectories

### 3.2.1 Space-for-time substitution

To compensate for the lack of GEDI’s historical record, we use space-for-time substitution method [37] to estimate AGBD recovery trend. Space-for-time is a technique to infer temporal trends by studying sites of different ages since some initial event, in our case samples with different post-fire recovery times [26]. Space-for-time relies on the assumption that the sites are similar enough so that the time since the disturbance is the most significant factor influencing the vegetation state. This assumption can easily be violated and fail to produce correct succession trajectories [26]. To justify and validate the use of space-for-time substitution in our forest samples, we compare ground-truth of NDVI recovery (from 35 years of Landsat NDVI data) to NDVI chronosequences generated by space-for-time substitution.

### 3.2.2 NDVI recovery reconstruction

We analyze NDVI recovery on the same dataset of filtered GEDI shots that’s used throughout the study. We generated NDVI recovery trajectories in two ways:

1. **Time series analysis:** For each burned pixel, we obtained the mean annual NDVI value for each year from 1985 to 2020. All the time series were aligned according to the year in which they burned and aggregated to create a time series of medians. We calculated % of NDVI change relative to the pre-fire NDVI for each age group. This time series analysis represents the “ground truth” for NDVI rate of recovery.
2. **Space-for-time substitution:** We generate chronosequences of NDVI and compare them to the ground truth recovery. Instead of using the entirety of NDVI time series for each pixel, we use NDVI values from 2019 to 2022, to correspond exactly to the GEDI sample year. We evaluate two chronosequences: one for absolute NDVI and one for relative NDVI. To compute relative NDVI, we use NDVI values one year prior to fire as control.

Our results (Section 4.1) showed that space-for-time is much more effective at reconstructing relative NDVI trajectories, emphasizing the importance of controls.

## 3.3 Burn area counterfactuals of biomass

As NDVI space-for-time demonstrated greater effectiveness when working with relative measurements, we decided to apply the same approach to analyze biomass recovery. Instead

of looking at raw AGBD values, we reconstructed AGBD recovery trajectory looking at the relative AGBD, defined as:

$$AGBD_{rel} = \frac{AGBD_{measured}}{AGBD_{control}} \quad (3.1)$$

We define control AGBD as the value of biomass density that the forest would have if it didn't burn, similar to the notion of carbon counterfactual in carbon credits [49]. The important question arises: as the mere choice of control can alter our results, how do we know our control is good enough? In response, we develop a framework for quantifying the quality of controls on unburned areas as placebos.

### 3.3.1 Using unburned areas as placebos for validation of controls

We use unburned areas as our placebo samples. To evaluate the quality of controls, we simulate many different “fake fires” on unburned areas, and calculate *RMSE* and  $R_2$  errors between proposed counterfactuals and actual GEDI AGBD measurements. Each fake fire is represented with a circle. We simulate many different fire sizes, sampling from the historic fire size distribution derived from MTBS perimeters. We then rank the proposed counterfactual-finding algorithms based on their accuracy.

#### Algorithms for Finding Counterfactuals

We implemented and evaluated several different algorithms for finding controls, many of which are used in existing studies [24, 45, 32]. Algorithms can be sorted into three broad categories:

1. Random or nearest neighbor sampling from the unburned areas surrounding the fire.
2. Using K-Means unsupervised clustering [19] (implemented using scikit Mini-Batch K-means [5]) to find similar forests, and sample controls from the unburned regions that belong to the same cluster.
3. Our approach - use random forests (RF) trained on unburned areas to predict synthetic AGBD values.

We tested several different variations of these algorithms. The performance of each approach is presented in the results section. We proceed to describe the random forest approach in more detail, as that one yielded convincingly best results.

## 3.4 Using Random Forests to Predict Aboveground Biomass from Landsat and Terrain Data

To create AGBD counterfactuals, we use random forest regressors with bagging to predict future biomass from multispectral Landsat and terrain data from the past. We train the models on unburned areas, and later use them to predict counterfactual biomass values for burned areas, based on their spectral signatures prior to fire. We train 35 separate random forest models, one for each year between 1985 and 2020. Each model is trained specifically for a single fire year  $y$ ; let's label each model correspondingly as  $rfm_y$ .

### 3.4.1 Selecting calibration data

The dependent variable is the AGBD value from GEDI's product Level 4A, representing aboveground biomass density. For calibration, we selected high-quality GEDI shots from unburned areas (as described in section 2.2). Each AGBD measurement was log-transformed, as we measured our final accuracy with root mean squared logarithmic error (RMSLE).

For independent variables we use Landsat multitemporal metrics and terrain measurements, which have been shown effective at predicting canopy heights [40]. For each model  $rf_i$ , we use 5 years of Landsat data from  $i - 5$  to  $i - 1$  (inclusive) as features. Each year of Landsat data included the annual mean for each optical band, and mean NDVI value. Terrain and soil features included slope, aspect, elevation as continuous, and soil type as a categorical variable. To incorporate a spatial component, each continuous feature is the focal average of values from 3x3 pixels surrounding the shot. Note that since we train one RF model for each year in the past, our Landsat predictive variables are sampled from different Landsat satellites (5, 7, 8 or a combination), depending on the satellite availability. Full list of features is presented in 3.1.

#### Spatial Auto-correlation

Forests exhibit biomass spatial auto-correlation, which can result in overestimation of model's predictive power [39]. Ideally, the test dataset should not contain samples that are geographically close to the samples in the training set, because they may be too similar to each other for reasons that are not captured in the independent variables. To reduce the impact of spatial auto-correlation, we divided the entire region of interest into 5km x 5km cells. We then randomly assign each cell to the training, or testing data set, using 15% to 85% split. Once

### 3.4 Using Random Forests to Predict Aboveground Biomass from Landsat and Terrain Data

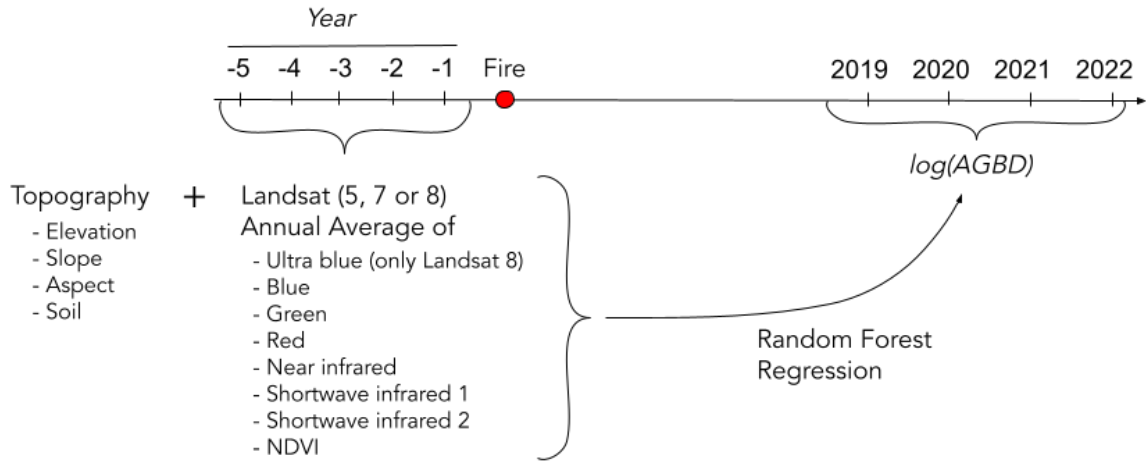


**Fig. 3.1** – Each random forest uses topography data with 5 years of consecutive, historic Landsat data, to predict  $\log(\text{AGBD})$  sampled from GEDI.

the cell is assigned to a dataset, all samples from that cell are assigned to the same split i.e. we train or test on the entire cells.

#### 3.4.2 Random forest training

Each random forest was trained with 5 years of Landsat data and a single set of terrain data, resulting in 36 (for Landsat 8) or 32 (for Landsat 5 and 7) predictive variables. We used out of bag [15] validation error to fine-tune model parameters 3.1, and we optimized the model for  $\log RMSE$ . We trained the models using fastai and scikit learn python libraries.

**Table 3.1** – Random forest regression parameters

Scikit Parameter	Value	Description
n_estimators	100	Number of trees
max_samples	0.85	Fraction of total samples to draw to train each tree.
max_features	0.5	Fraction of total features to sample at each split point.
min_samples_leaf	30	The minimum number of samples in a leaf node.

#### 3.4.3 Random forest inference

At inference time, for each burned sample we find a corresponding random forest model based on the year in which the sample area burned. If the sample fire year was in 1990 for example, we run inference using the model  $rfm_{1990}$ , and record the predicted AGBD value as the sample counterfactual.

### 3.5 Code and data availability

All data sources used in this study are free and publicly available. Links to all sources and libraries are in the References section, and on the github project page. Code is available at <https://github.com/mahuna13/fire-regen/releases/tag/v0.1.0>.

# Chapter 4

## Results

### 4.1 Validation of space-for-time substitution using NDVI historic data

In this section we address the following questions:

1. Can the space-for-time substitution on our dataset produce accurate reconstruction of long-term recovery?
2. Is space-for-time substitution better at estimating relative or absolute recovery?

Figure 4.1 compares reconstructed space-for-time chronosequences with the ground-truth obtained using time series analysis. We compared chronosequences of medians across 34 years of post-fire recovery. Our results show that the reconstruction of relative NDVI recovery is significantly better ( $R^2 = 0.84$ ) than the reconstruction of absolute NDVI values ( $R^2 = 0.21$ ). Few years in the reconstruction time series have large variability (Figure A.3). We assume that vegetation recovery should be a relatively smooth function in the absence of additional disturbances, and we apply sliding window weighted average (weighted by the number of samples per recovery year) to obtain the final trajectory, achieving the accuracy of  $R^2 = 0.91$ . Space-for-time reconstruction for relative NDVI preserves the overall shape and rate of recovery — especially during the earlier years when more data is available.

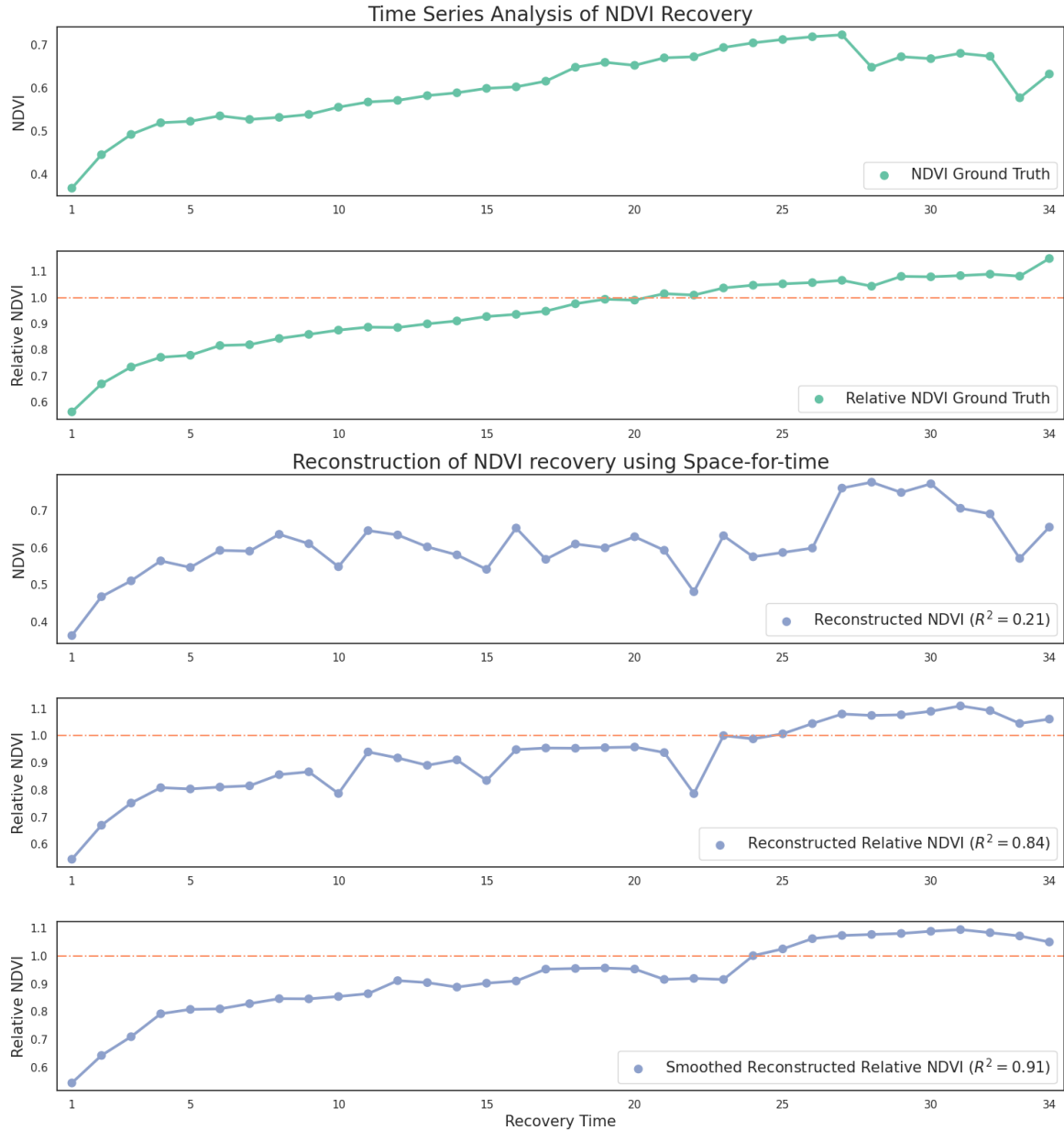


**Fig. 4.1** – Comparing the medians of ground-truth NDVI recovery time-series (top two plots), with reconstructed space-for-time NDVI trajectories (bottom three). Space-for-time yields a much higher accuracy when reconstructing relative ( $R^2 = 0.84$ ) than absolute ( $R^2 = 0.21$ ) NDVI recovery.

## 4.2 Evaluation of controls on unburned areas

Previous section demonstrates the importance of controls when implementing space-for-time substitution to estimate recovery. Since we don't have pre-fire AGBD values to use for control, we instead use counterfactuals. We implemented numerous algorithms for calculating AGBD

counterfactuals and evaluated them on unburned areas as placebos. The results of comparing them against GEDI AGBD values as ground truth are presented in the table 4.1. Our random forest regression yielded the highest accuracy with  $R^2$  of 0.57.

**Table 4.1** – Evaluation of AGBD counterfactual-finding algorithms on placebos

Algorithm	Accuracy	
	RMSE	$R^2$
Mean of 200 unburned shots around 5k fire perimeter	127.80	0.1
Mean of 200 unburned shots around 3k fire perimeter	120.98	0.13
Mean of 500 unburned shots around 1k fire perimeter	118.12	0.15
Mean of 200 closest unburned pixels	114.25	0.11
Terrain clustering	125.61	0.12
4 year pre-fire NDVI clustering	126.41	0.18
4 year LANDSAT all bands + NDVI clustering	103.03	0.28
Clustering based on RF-selected terrain and spectral variables	109.5	0.30
Synthetic RF Counterfactual	88.72	0.57

## 4.3 Post-fire NDVI and AGBD recovery

### 4.3.1 NDVI recovery using time series analysis

The results of the NDVI time series analysis demonstrate consistent post-fire recovery trends, as shown in Figure 4.2. Approximately 80% of forest samples have fully recovered after 32 years, where full recovery is defined as the return to its pre-fire levels. After 21 years of recovery, over 50% of the samples have reached their pre-disturbance values.

Prior to a fire, NDVI values exhibit relative stability, with an interquartile range (IQR) of approximately 0.15. However, immediately after a fire, there is a notable increase in variability, indicated by an IQR of 0.36. This heightened variability decreases steadily over time, reaching its pre-fire spread after 20 years of recovery.

One year following the fire, NDVI reaches its minimum value and subsequently begins to increase, eventually surpassing the pre-fire values. After 30 years, median NDVI is 7.1% higher than the pre-fire value. Density plot in Figure 4.3 shows the progression of recovery over the three decades post-fire.

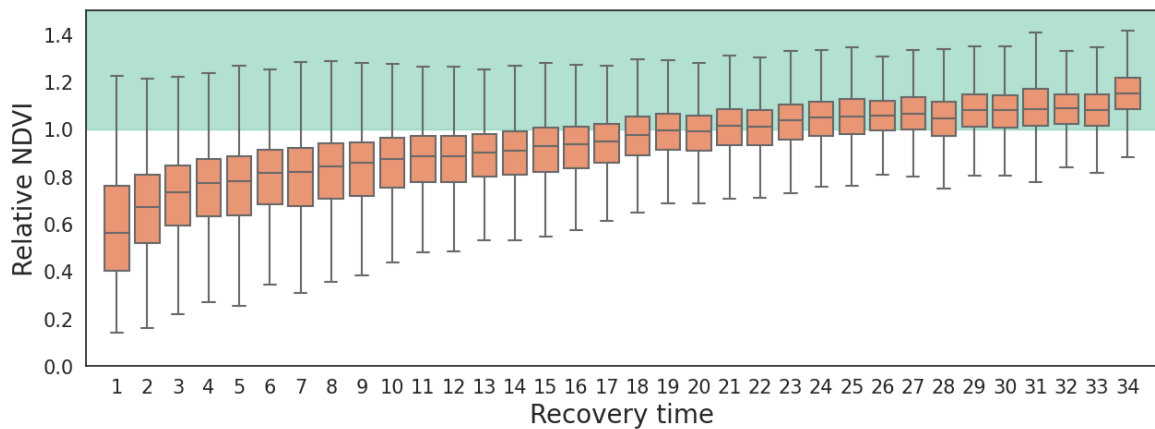


**Fig. 4.2** – NDVI recovery time series relative to its pre-fire value. Green shaded area represents full recovery, where relative NDVI  $> 1$ . NDVI surpasses its pre-fire values after approximately 25 years.

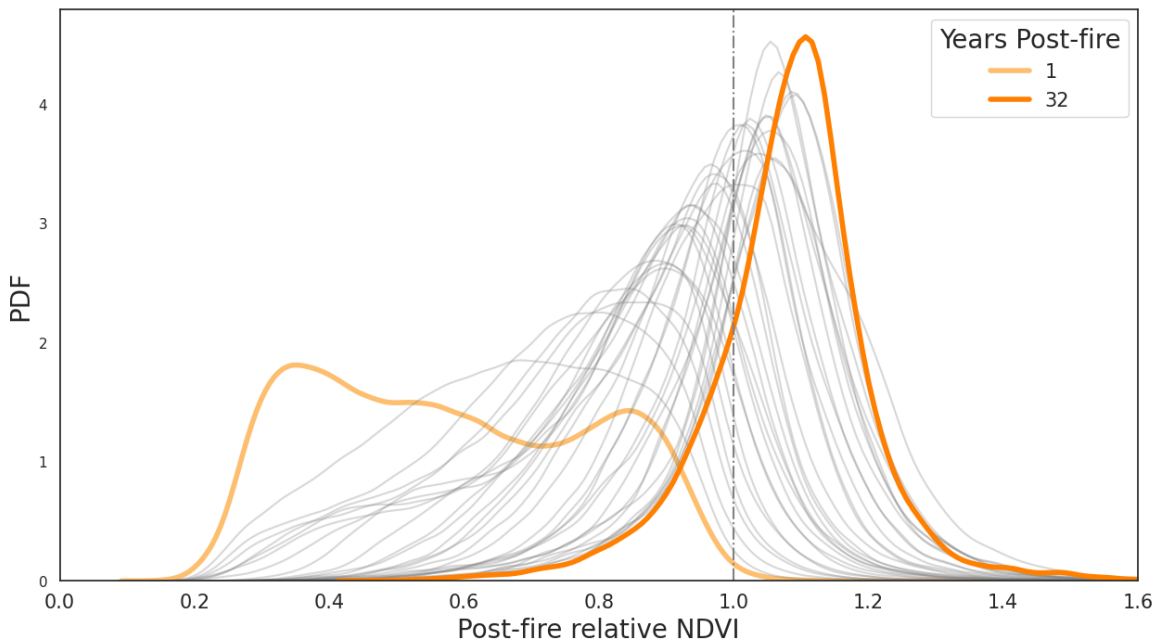


**Fig. 4.3** – Progression of relative NDVI density from 1 year to 32 years post-fire.

### 4.3.2 Aboveground biomass recovery using space-for-time analysis

We use space-for-time substitution to estimate post-fire AGBD recovery. Relative AGBD value is calculated with respect to the RF-derived counterfactual AGBD, discussed in section 4.3. Absolute and relative AGBD values for each year have a large spread, and contain many outliers (Figure A.9). Similarly to NDVI, the spread generally reduces as the recovery time

increases. To interpret the general recovery trend, we look at median values of the relative AGBD time series after applying weighted average smoothing (Figure 4.4).

In the first 6 years following a fire, we see a continued decrease in biomass density, from 71% of control AGBD value to 47%. In the period of 8 to 23 years of recovery, we see a relatively stable biomass measurements between 50 and 55%. We observe another drop in biomass around the 25th year of recovery. Finally, we only start to see a pattern resembling one of recovery around the year 27. In the last 10 years of the chronosequence, we see an upward recovery trajectory that regains more than 20% of lost biomass, increasing from 45% to 66% of its relative value.

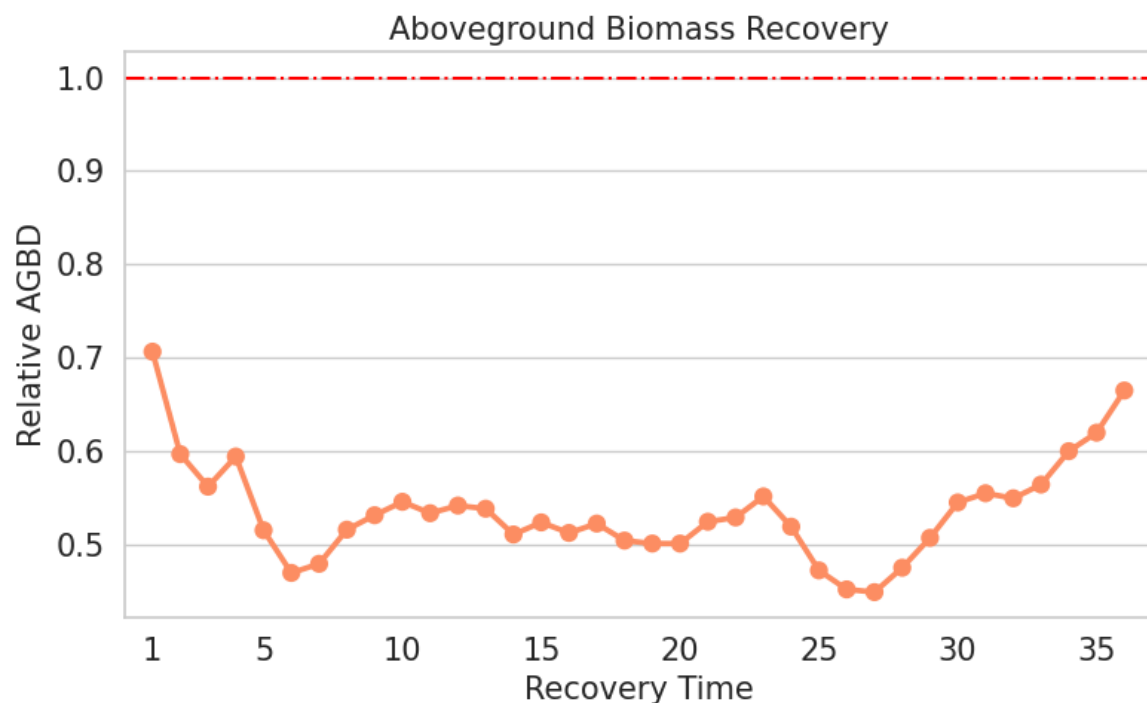


**Fig. 4.4** – Post-fire AGBD recovery over 35 years, characterized by initial decline, a period of stability, and eventual recovery trend starting around 25 years after fire.

### 4.3.3 Effects of severity on vegetation recovery

We separated recovery trajectories based on the burn severity into three categories: low, medium and high. We observe markedly different trends between NDVI and AGBD recovery. The extent of NDVI and AGBD losses is influenced by the severity of the fire, with higher severity resulting in larger overall losses. There is a clear separation and ordering between areas that burned at low, medium and high severity, that is preserved throughout the initial recovery period. Eventually, values in all severity categories start converging for both NDVI

and AGBD. Notably, immediate post-fire AGBD losses for low severity burns are negligible. We further demonstrate this in the following results section, and discuss the reasons and implications of it in the Discussion. It's worth noting that the number of samples, and consequently the confidence of estimates, decreases for larger recovery periods.

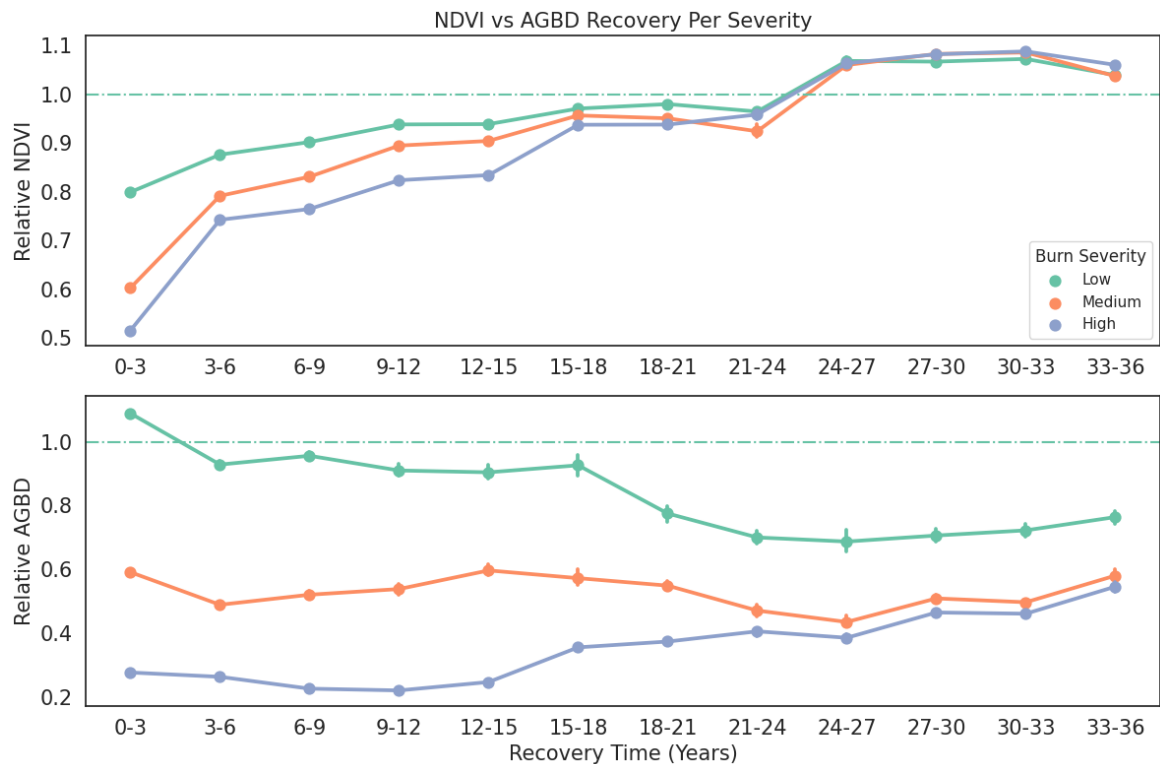


**Fig. 4.5 – Post-fire vegetation recovery per severity category.** Top plot shows NDVI, bottom plot shows AGBD trajectories. NDVI reaches full recovery by the year 25, while biomass is much slower to recover.

All NDVI severity categories eventually recover and reach their pre-fire values within 25 years of recovery (Table 4.2). The most rapid recovery rate occurs in the first 5 years of recovery in high severity areas, where the vegetation regains 26.8% of its initial NDVI value in 4 years. Post-fire NDVI values continue to increase after reaching a full recovery of 100% in all severity categories.

Unlike NDVI, AGBD does not recover in any of the severity categories after 35 years, with notably different trends for each burn severity:

- In low severity areas, we observe stable biomass levels without significant post-fire loss in the first 15 years of recovery. This is followed by a downward trend, period of stability and finally potential recovery trend near the end of the time series.

**Table 4.2** – Mean post-fire NDVI as % of pre-fire NDVI

Severity	Number of recovery years							
	1	5	10	15	20	25	30	34
Low	79.5%	86.3%	93.6%	96.6%	101.2%	104.6%	107.7%	118.0%
Medium	57.0%	75.0%	86.7%	91.8%	97.6%	103.7%	106.1%	109.2%
High	39.0%	65.8%	78.4%	87.2%	96.0%	105.1%	107.4%	104.1%
All	58.0%	74.8%	84.9%	90.9%	97.8%	104.6%	107.1%	115.5%

- Medium severity areas remain relatively stable throughout the recovery period.
- High severity areas exhibit initial decline, followed by an upward recovery trend. Biomass values nearly double in the last 20 years of recovery.

Areas that burned at high severity are the only ones for which we observe a clear and consistent recovery trend. Since our data contains many outliers and diverse variance, we fit a polynomial function only to the medians in each age group ( $R^2 = 0.897$ ), similar to the approach used in [22]. By extrapolating the polynomial fit, we conclude that if the same recovery trend continues, high severity areas would reach the point of full biomass recovery 54 years after fire.

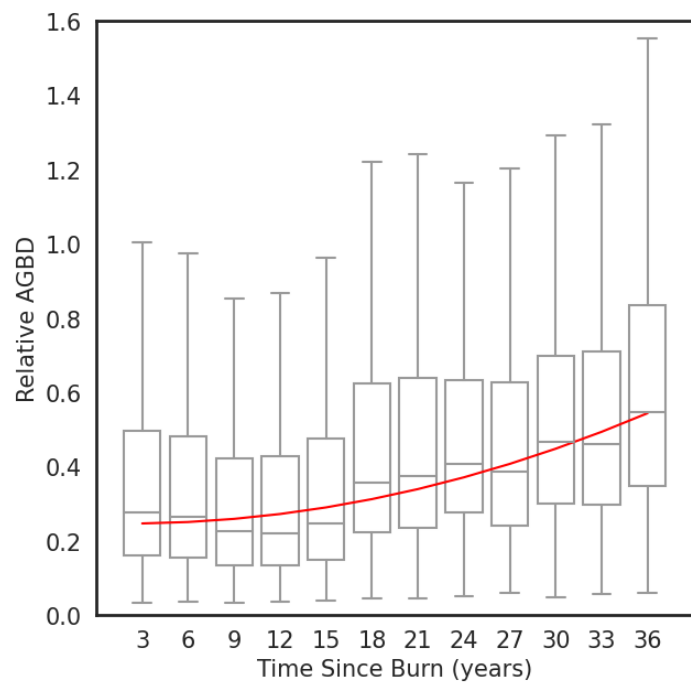


**Fig. 4.6** – Boxplot of AGBD recovery in high burn severity areas. Red line is a second degree polynomial fit ( $R^2 = 0.897$ ) to medians in each 3-year age bucket.

# **Chapter 5**

## **Discussion**

### **5.1 Post-fire Recovery**

In this study, our focus was on the long-term (over 30 years) recovery of forests in the Sierra Nevada region following a fire. We utilize space-for-time substitution with synthetic biomass controls to reconstruct and compare the post-fire loss and regrowth of Landsat NDVI and GEDI AGBD. Our findings indicate a more rapid and significant recovery of NDVI compared to AGBD. NDVI reaches full recovery after 25 years, while biomass reaches the 68% level after 35 years of recovery.

These results align with the previous findings from boreal forests that foliage growth recovers at a faster pace than biomass accumulation [12, 13]. Our AGBD trajectories exhibit similarities to the canopy height trajectories found in [32], including a concave shape in high-severity burns, biomass decline during the initial recovery phase, and a delayed increase in biomass after several decades. However, our findings contradict the results of a study conducted in the Pacific Northwest that predicted a downward biomass trend in high-severity areas [24]. We speculate that this discrepancy may stem from the choice of controls, as the aforementioned study used randomly selected unburned regions around the fire perimeter, which yielded the lowest accuracy in our placebo tests.

GEDI's biomass measurements are sensitive to the changes in mid and higher canopy heights. Consequently, after low severity fires, which are often classified as surface fires, GEDI does not detect statistically significant biomass changes. Our additional experiments on 2019-2022 fires demonstrate this further - see section A.2. Additionally, as observed in our recovery results, GEDI may not be able to capture initial recovery in low and medium severity patches. The reason for this may be that low and medium severity fires typically preserve a greater number of standing trees, and it takes time for new growth to reach the canopy heights that GEDI can detect. On the other hand, GEDI is more sensitive to the loss

and recovery occurring in areas with higher burn severity. In these areas, a significant portion of the vegetation has perished, resulting in a shortening of the canopy. As a result, AGBD recovery trends are most easily observed in the high severity category.

## 5.2 Space-for-time Substitution with Counterfactuals

In this work we show the advantages of using space-for-time to reconstruct relative measurement, rather than absolute. Study [32] used relative measures of canopy heights with space-for-time analysis, in the hopes of reducing spatial bias introduced by different growing conditions across geographical sites. Our results endorse this intuition, as the reconstruction of relative signal yielded superior accuracy.

To calculate relative values, a suitable control is essential. In the study of burned areas, various controls have been employed [21, 42, 45, 32, 24]. Our results emphasize the importance of careful control selection, as different choices can lead to significantly divergent outcomes. We also demonstrate that controls incorporating spectral similarities between forests yield superior performance in placebo tests. Furthermore, setting up placebo tests in unburned areas is relatively straightforward and can provide valuable insights for control evaluation. Encouraging the adoption of such practices would be highly beneficial.

## 5.3 Limitations

During our analysis, we noticed discrepancies between GEDI and optical data. While they may come from inaccuracies in the optical data, some of it could stem from GEDI’s geolocation error. As forests of Sierra Nevada can be sparse or fragmented (see an example aerial image A.5), 10m geolocation error may introduce greater inaccuracies than when sampling in dense tropical forests. Moreover, lidars tend to perform poorly on steep slopes, which are common in our region of interest, potentially introducing additional errors [46]. Additionally, understanding how GEDI measurements work on fire-affected vegetation requires further investigation, although our study contributes to this effort. These potential limitations should be addressed in future work or field studies. Additional limitations come from the use of optical data, and are further explained in the appendix section A.1.

Notably, the RMSE remains relatively high (88.72) even for the best-performing counterfactual (4.1), compared to the mean AGBD value in unburned areas of 123.55 Mg/ha. We would likely achieve better results by augmenting our ML model to include a more comprehensive set of Landsat temporal data, similar to what was used by Potapov in [40], which is left for future work.

# References

- [1] (2022a). Google earth engine landsat collections. <https://developers.google.com/earth-engine/datasets/catalog/landsat>.
- [2] (2022a). Landsat collection 2. <https://www.usgs.gov/landsat-missions/landsat-collection-2>.
- [3] (2022b). Landsat normalized difference vegetation index. <https://www.usgs.gov/landsat-missions/landsat-normalized-difference-vegetation-index>.
- [4] (2022b). Nasa srtm digital elevation 30m. [https://developers.google.com/earth-engine/datasets/catalog/USGS\\_SRTMGL1\\_003](https://developers.google.com/earth-engine/datasets/catalog/USGS_SRTMGL1_003).
- [5] (2022). Scikit mini-batch k-means clustering. <https://scikit-learn.org/stable/modules/generated/sklearn.cluster.MiniBatchKMeans.html>.
- [6] (2022c). Us lithology. [https://developers.google.com/earth-engine/datasets/catalog/CSP\\_ERGo\\_1\\_0\\_US\\_lithology](https://developers.google.com/earth-engine/datasets/catalog/CSP_ERGo_1_0_US_lithology).
- [7] (2022d). Usfs landscape change monitoring system v2021.7. [https://developers.google.com/earth-engine/datasets/catalog/USFS\\_GTAC\\_LCMS\\_v2021-7](https://developers.google.com/earth-engine/datasets/catalog/USFS_GTAC_LCMS_v2021-7).
- [8] Abatzoglou, J. T. and Williams, A. P. (2016). Impact of anthropogenic climate change on wildfire across western US forests. *Proceedings of the National Academy of Sciences*, 113(42):11770–11775. Publisher: Proceedings of the National Academy of Sciences.
- [9] Anderegg, W. R. L., Trugman, A. T., Badgley, G., Anderson, C. M., Bartuska, A., Ciais, P., Cullenward, D., Field, C. B., Freeman, J., Goetz, S. J., Hicke, J. A., Huntzinger, D., Jackson, R. B., Nickerson, J., Pacala, S., and Randerson, J. T. (2020). Climate-driven risks to the climate mitigation potential of forests. *Science*, 368(6497):eaaz7005. Publisher: American Association for the Advancement of Science.
- [10] Badgley, G., Chay, F., Chegwidden, O. S., Hamman, J. J., Freeman, J., and Cullenward, D. (2022). California’s forest carbon offsets buffer pool is severely undercapitalized. *Frontiers in Forests and Global Change*, 5.
- [11] Balmford, A., Keshav, S., Venmans, F., Coomes, D., Groom, B., Madhavapeddy, A., and Swinfield, T. (2023). Realising the social value of impermanent carbon credits.
- [12] Bolton, D. K., Coops, N. C., Hermosilla, T., Wulder, M. A., and White, J. C. (2017). Assessing variability in post-fire forest structure along gradients of productivity in the Canadian boreal using multi-source remote sensing. *Journal of Biogeography*, 44(6):1294–1305. \_eprint: <https://onlinelibrary.wiley.com/doi/pdf/10.1111/jbi.12947>.

- [13] Bolton, D. K., Coops, N. C., and Wulder, M. A. (2015). Characterizing residual structure and forest recovery following high-severity fire in the western boreal of Canada using Landsat time-series and airborne lidar data. *Remote Sensing of Environment*, 163:48–60.
- [14] Carlson, T. N., Perry, E. M., and Schmugge, T. J. (1990). Remote estimation of soil moisture availability and fractional vegetation cover for agricultural fields. *Agricultural and Forest Meteorology*, 52(1):45–69.
- [15] Cutler, A., Cutler, D. R., and Stevens, J. R. (2012). Random Forests. In Zhang, C. and Ma, Y., editors, *Ensemble Machine Learning: Methods and Applications*, pages 157–175. Springer, New York, NY.
- [16] Dubayah, R., Blair, J. B., Goetz, S., Fatoyinbo, L., Hansen, M., Healey, S., Hofton, M., Hurt, G., Kellner, J., Luthcke, S., Armston, J., Tang, H., Duncanson, L., Hancock, S., Jantz, P., Marselis, S., Patterson, P. L., Qi, W., and Silva, C. (2020). The Global Ecosystem Dynamics Investigation: High-resolution laser ranging of the Earth’s forests and topography. *Science of Remote Sensing*, 1:100002.
- [17] Falkowski, M. J., Evans, J. S., Martinuzzi, S., Gessler, P. E., and Hudak, A. T. (2009). Characterizing forest succession with lidar data: An evaluation for the Inland Northwest, USA. *Remote Sensing of Environment*, 113(5):946–956.
- [18] Goetz, S. J., Fiske, G. J., and Bunn, A. G. (2006). Using satellite time-series data sets to analyze fire disturbance and forest recovery across Canada. *Remote Sensing of Environment*, 101(3):352–365.
- [19] Hartigan, J. A. and Wong, M. A. (1979). Algorithm AS 136: A K-Means Clustering Algorithm. *Journal of the Royal Statistical Society. Series C (Applied Statistics)*, 28(1):100–108. Publisher: [Wiley, Royal Statistical Society].
- [20] Healey, S. P., Yang, Z., Gorelick, N., and Ilyushchenko, S. (2020). Highly Local Model Calibration with a New GEDI LiDAR Asset on Google Earth Engine Reduces Landsat Forest Height Signal Saturation. *Remote Sensing*, 12(17):2840. Number: 17 Publisher: Multidisciplinary Digital Publishing Institute.
- [21] Hicke, J. A., Asner, G. P., Kasischke, E. S., French, N. H. F., Randerson, J. T., James Collatz, G., Stocks, B. J., Tucker, C. J., Los, S. O., and Field, C. B. (2003). Postfire response of North American boreal forest net primary productivity analyzed with satellite observations. *Global Change Biology*, 9(8):1145–1157. \_eprint: <https://onlinelibrary.wiley.com/doi/pdf/10.1046/j.1365-2486.2003.00658.x>.
- [22] Holcomb, A., Mathis, S., and Coomes, D. A. (2023). Fusing GEDI shots and annual forest change maps to estimate tropical forest recovery rates across the Amazon basin.
- [23] Iglesias, V., Balch, J. K., and Travis, W. R. (2022). U.S. fires became larger, more frequent, and more widespread in the 2000s. *Science Advances*, 8(11):eabc0020. Publisher: American Association for the Advancement of Science.
- [24] Ilangakoon, N., Balch, J. K., Nagy, R. C., and Iglesias, V. (2023). Postfire recovery of western US conifer forests (1984–2017) using space-borne lidar data. preprint, *Ecology*.

- [25] Ipcc, I. (2006). Guidelines for national greenhouse gas inventories. *Prepared by the National Greenhouse Gas Inventories Programme. Eggleston HS, Buendia L, Miwa K, Ngara T, Tanabe K, editors. Published: IGES, Japan.*
- [26] Johnson, E. A. and Miyanishi, K. (2008). Testing the assumptions of chronosequences in succession. *Ecology Letters*, 11(5):419–431. \_eprint: <https://onlinelibrary.wiley.com/doi/pdf/10.1111/j.1461-0248.2008.01173.x>.
- [27] K. Ingram, S. K. (2022). Natural history of the sierra nevada. <https://anrcatalog.ucanr.edu/Details.aspx?itemNo=8535#FullDescription>.
- [28] Keith, H., Vardon, M., Obst, C., Young, V., Houghton, R. A., and Mackey, B. (2021). Evaluating nature-based solutions for climate mitigation and conservation requires comprehensive carbon accounting. *Science of The Total Environment*, 769:144341.
- [29] Kellner, J. R., Armston, J., and Duncanson, L. (2023). Algorithm Theoretical Basis Document for GEDI Footprint Aboveground Biomass Density. *Earth and Space Science*, 10(4):e2022EA002516. \_eprint: <https://onlinelibrary.wiley.com/doi/pdf/10.1029/2022EA002516>.
- [30] Kennedy, R. E., Yang, Z., Cohen, W. B., Pfaff, E., Braaten, J., and Nelson, P. (2012). Spatial and temporal patterns of forest disturbance and regrowth within the area of the Northwest Forest Plan. *Remote Sensing of Environment*, 122:117–133.
- [31] Liang, M., Duncanson, L., Silva, J. A., and Sedano, F. (2023). Quantifying aboveground biomass dynamics from charcoal degradation in Mozambique using GEDI Lidar and Landsat. *Remote Sensing of Environment*, 284:113367.
- [32] Lin, S., Zhang, H., Liu, S., Gao, G., Li, L., and Huang, H. (2023). Characterizing Post-Fire Forest Structure Recovery in the Great Xing'an Mountain Using GEDI and Time Series Landsat Data. *Remote Sensing*, 15(12):3107. Number: 12 Publisher: Multidisciplinary Digital Publishing Institute.
- [33] Meng, R., Dennison, P. E., Huang, C., Moritz, M. A., and D'Antonio, C. (2015). Effects of fire severity and post-fire climate on short-term vegetation recovery of mixed-conifer and red fir forests in the Sierra Nevada Mountains of California. *Remote Sensing of Environment*, 171:311–325.
- [34] Milenković, M., Reiche, J., Armston, J., Neuenschwander, A., De Keersmaecker, W., Herold, M., and Verbesselt, J. (2022). Assessing Amazon rainforest regrowth with GEDI and ICESat-2 data. *Science of Remote Sensing*, 5:100051.
- [35] Miller, J. D. and Thode, A. E. (2007). Quantifying burn severity in a heterogeneous landscape with a relative version of the delta Normalized Burn Ratio (dNBR). *Remote Sensing of Environment*, 109(1):66–80.
- [36] Parks, S. A., Holsinger, L. M., Voss, M. A., Loehman, R. A., and Robinson, N. P. (2018). Mean Composite Fire Severity Metrics Computed with Google Earth Engine Offer Improved Accuracy and Expanded Mapping Potential. *Remote Sensing*, 10(6):879. Number: 6 Publisher: Multidisciplinary Digital Publishing Institute.

- [37] Pickett, S. T. A. (1989). Space-for-Time Substitution as an Alternative to Long-Term Studies. In Likens, G. E., editor, *Long-Term Studies in Ecology: Approaches and Alternatives*, pages 110–135. Springer, New York, NY.
- [38] Picotte, J. J., Bhattacharai, K., Howard, D., Lecker, J., Epting, J., Quayle, B., Benson, N., and Nelson, K. (2020). Changes to the Monitoring Trends in Burn Severity program mapping production procedures and data products. *Fire Ecology*, 16(1):16.
- [39] Ploton, P., Mortier, F., Réjou-Méchain, M., Barbier, N., Picard, N., Rossi, V., Dormann, C., Cornu, G., Viennois, G., Bayol, N., Lyapustin, A., Gourlet-Fleury, S., and Pélissier, R. (2020). Spatial validation reveals poor predictive performance of large-scale ecological mapping models. *Nature Communications*, 11(1):4540. Number: 1 Publisher: Nature Publishing Group.
- [40] Potapov, P., Li, X., Hernandez-Serna, A., Tyukavina, A., Hansen, M. C., Kommareddy, A., Pickens, A., Turubanova, S., Tang, H., Silva, C. E., Armston, J., Dubayah, R., Blair, J. B., and Hofton, M. (2021). Mapping global forest canopy height through integration of GEDI and Landsat data. *Remote Sensing of Environment*, 253:112165.
- [41] Pugh, T. A. M., Arneth, A., Kautz, M., Poulter, B., and Smith, B. (2019). Important role of forest disturbances in the global biomass turnover and carbon sinks. *Nature Geoscience*, 12(9):730–735. Number: 9 Publisher: Nature Publishing Group.
- [42] Reed, R. A., Finley, M. E., Romme, W. H., and Turner, M. G. (1999). Aboveground Net Primary Production and Leaf-Area Index in Early Postfire Vegetation in Yellowstone National Park. *Ecosystems*, 2(1):88–94.
- [43] Saarela, S., Holm, S., Healey, S. P., Andersen, H.-E., Petersson, H., Prentius, W., Patterson, P. L., Næsset, E., Gregoire, T. G., and Ståhl, G. (2018). Generalized Hierarchical Model-Based Estimation for Aboveground Biomass Assessment Using GEDI and Landsat Data. *Remote Sensing*, 10(11):1832. Number: 11 Publisher: Multidisciplinary Digital Publishing Institute.
- [44] Seddon, N., Chausson, A., Berry, P., Girardin, C. A. J., Smith, A., and Turner, B. (2020). Understanding the value and limits of nature-based solutions to climate change and other global challenges. *Philosophical Transactions of the Royal Society B: Biological Sciences*, 375(1794):20190120. Publisher: Royal Society.
- [45] Serra-Burriel, F., Delicado, P., Prata, A. T., and Cucchietti, F. M. (2021). Estimating heterogeneous wildfire effects using synthetic controls and satellite remote sensing. *Remote Sensing of Environment*, 265:112649.
- [46] Simard, M., Pinto, N., Fisher, J. B., and Baccini, A. (2011). Mapping forest canopy height globally with spaceborne lidar. *Journal of Geophysical Research: Biogeosciences*, 116(G4). \_eprint: <https://onlinelibrary.wiley.com/doi/10.1029/2011JG001708>.
- [47] Steiner, J. L., Wetter, J., Robertson, S., Teet, S., Wang, J., Wu, X., Zhou, Y., Brown, D., and Xiao, X. (2020). Grassland Wildfires in the Southern Great Plains: Monitoring Ecological Impacts and Recovery. *Remote Sensing*, 12(4):619. Number: 4 Publisher: Multidisciplinary Digital Publishing Institute.

- [48] Tanase, M., de la Riva, J., Santoro, M., Pérez-Cabello, F., and Kasischke, E. (2011). Sensitivity of SAR data to post-fire forest regrowth in Mediterranean and boreal forests. *Remote Sensing of Environment*, 115(8):2075–2085.
- [49] West, T. A. P., Börner, J., Sills, E. O., and Kontoleon, A. (2020). Overstated carbon emission reductions from voluntary REDD+ projects in the Brazilian Amazon. *Proceedings of the National Academy of Sciences*, 117(39):24188–24194. Publisher: Proceedings of the National Academy of Sciences.



# **Appendix A**

## **Supplementary Information**

### **A.1 Limitations of optical data**

Although our results indicate that NDVI reaches full recovery, this measure alone does not fully capture the extent of forest regeneration due to NDVI's propensity for saturation. Additionally, NDVI lacks the ability to accurately distinguish between different vegetation types or species. In the aftermath of a fire in the Sierras, shrubs often compete with tree species, and an area dominated by shrubs can exhibit the same NDVI values as a forested area, despite representing a significantly different ecosystem with distinct biomass content compared to the pre-fire condition.

Another limitation of optical data is with its ability to distinguish severity categories. While the MTBS burn severity dataset has been used extensively for a variety of fire research in the US, several limitations have been previously noted. Thresholds for low, medium and high burn severity have been criticized as subjective and not validated sufficiently on vegetation field data, while dNBR and rdNBR indices have exhibited different levels of accuracy when compared to CBI in different geographical locations. Furthermore, direct comparison of severity categories across fires might not be appropriate, and in the future dNBR offsets should be applied. Finally, optical indeces can underestimate burn areas in low and medium burn severity, as they have limited visibility into the affected understory.

Land cover classification used in this study - LCSM, does not divide categories based on the species representation. As a result, we can't differentiate between deciduous and evergreen forests, or forest dominated by red fir or mixed conifer. Species composition can influence fire impacts [33], and in a future study biomass response could be analyzed for different forest types.

## A.2 GEDI detects statistically significant carbon losses in areas of medium and high burn severity, but not in low burn severity

We analyzed differences in AGBD between pre-fire and post-fire GEDI measurements on fires that burned at the time of GEDI collection - from 2019 to 2022. GEDI does not detect statistically significant carbon changes in areas of low burn severity. Since AGBD loss in low severity areas is normally distributed, as seen in A.1, we can use paired ttest to evaluate if measurements from before and after fire are significantly different from each other. Paired ttest on four large Sierra Nevada fires (Castle, Creek, North Complex and Windy) showed pvalues larger than 0.05 for low severity fires, and pvalues were effectively zero for medium and high severity fires (Table A.1). The analysis demonstrates that GEDI does not detect significantly significant difference between AGBD values pre and AGBD values post fire, in low burn severity areas.

**Table A.1** – Paired ttest on before and after AGBD measurements

Fire Name	Ttest pvalue		
	Low Severity	Medium Severity	High Severity
Castle (2020)	0.24	0.0	0.0
Creek (2020)	0.11	0.0	0.0
North Complex (2020)	0.22	0.0	0.0
Windy (2021)	0.229	0.00044	0.0

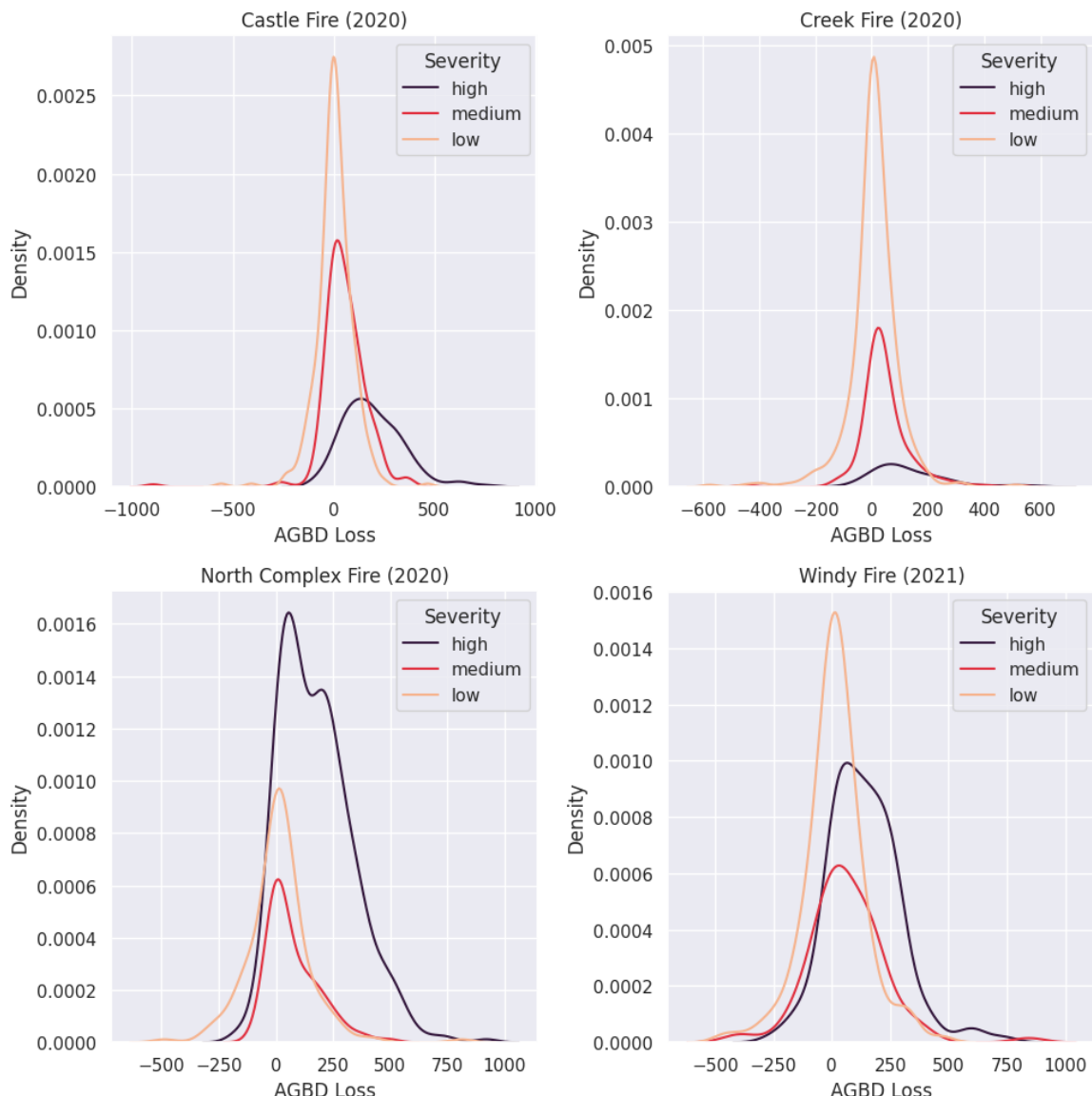


**Fig. A.1** – Density curves for AGBD loss for 4 separate fires, per burn severity.

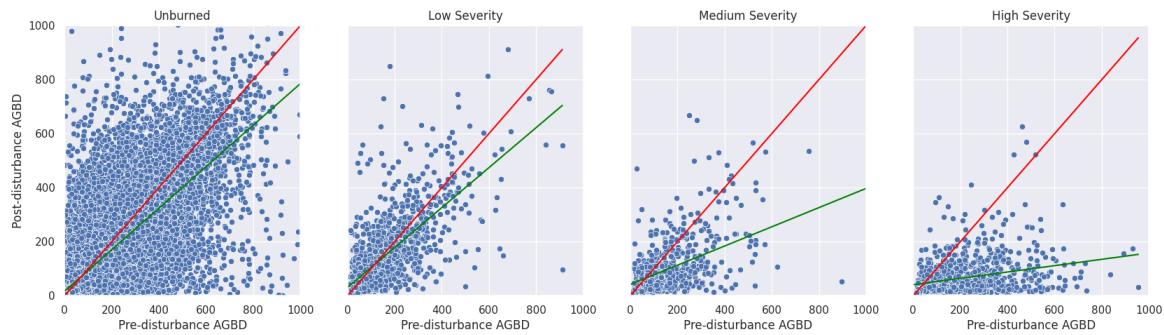


**Fig. A.2** – Each plot shows a regression between coincident (geo coordinates within 20m of each other) GEDI shots for AGBD measurements before and after fires. Plots are presented in this order, from left to right: unburned, low severity, medium severity and high severity burns. Red line is a  $y=x$  line, while green line represents the best linear regression fit for the corresponding plot.

## A.3 Supplementary Figures

### A.3.1 Validation of space-for-time substitution using NDVI historic data

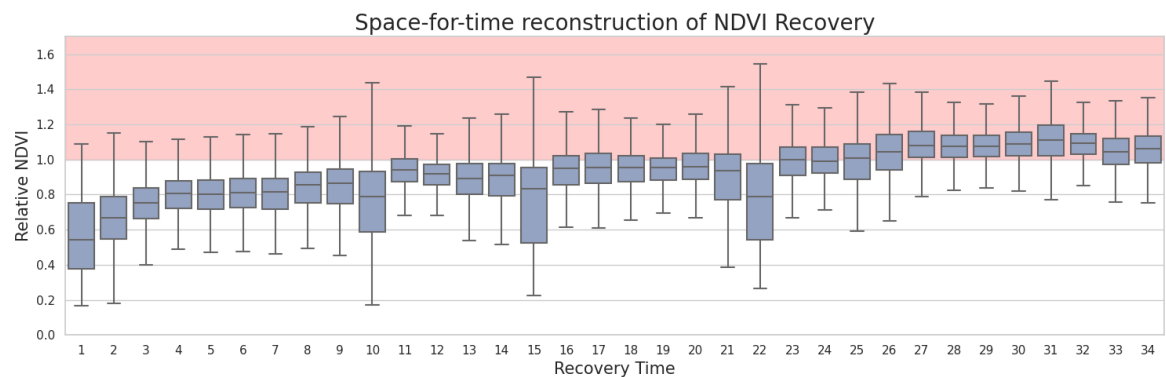


**Fig. A.3** – A boxplot showing relative NDVI reconstructed using space-for-time substitution. The trend looks comparable to the ground-truth NDVI, aside for years 10, 15, 21 and 22 that show a wide spread.

### A.3.2 NDVI Recovery

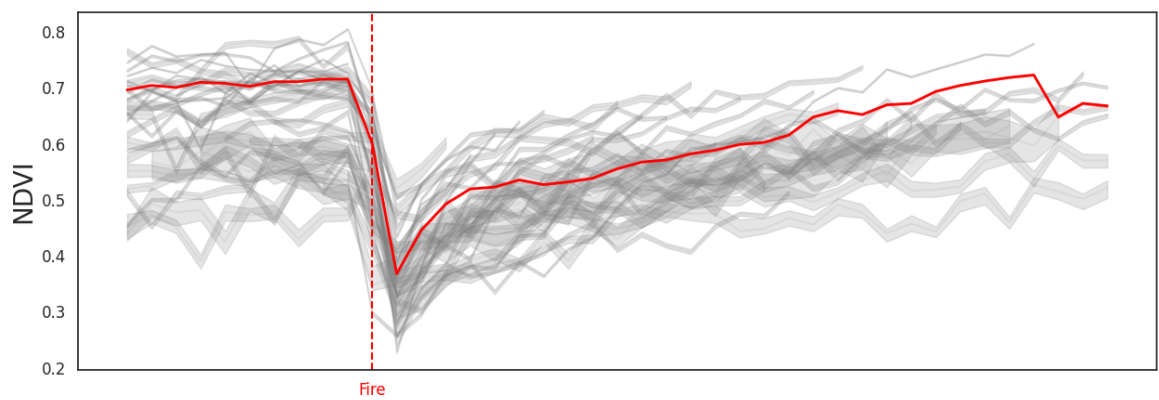


**Fig. A.4** – A visual representation of the NDVI recovery trajectories across all examined fire years (1984-2020).

### A.3.3 GEDI geolocation error



**Fig. A.5** – This aerial image of Sierra Nevada forest shows how sparse and fragmented these forests can be, representing a potential challenge for GEDI's geolocation error of 10m.

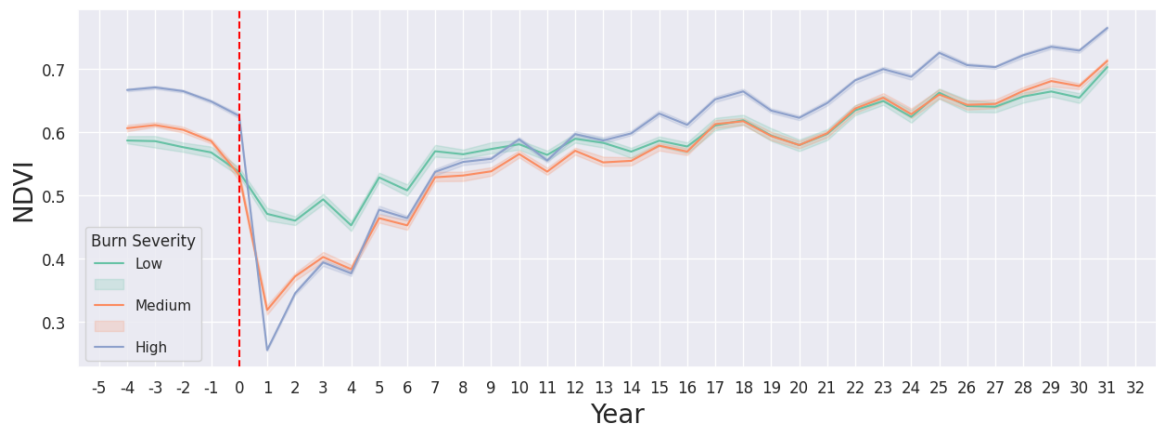


**Fig. A.6** – Time series of NDVI recovery for a single fire year - 1988, by severity. Larger NDVI losses occur in higher burn severity, but all three NDVI trajectories recover to their initial values, and beyond.



**Fig. A.7 – Space-for-time NDVI recovery trajectories.** Top: Raw NDVI values from 2019 to 2022. Middle: Control NDVI value sampled one year before the fire. Bottom: Relative NDVI representing the ratio of raw NDVI and control NDVI. Relative NDVI values exhibit clear recovery patterns that match the ground truth recovery estimates; the bottom graph is the only one where clear separation between fire severities is visible. The outliers are caused by the lack of samples for those recovery years.

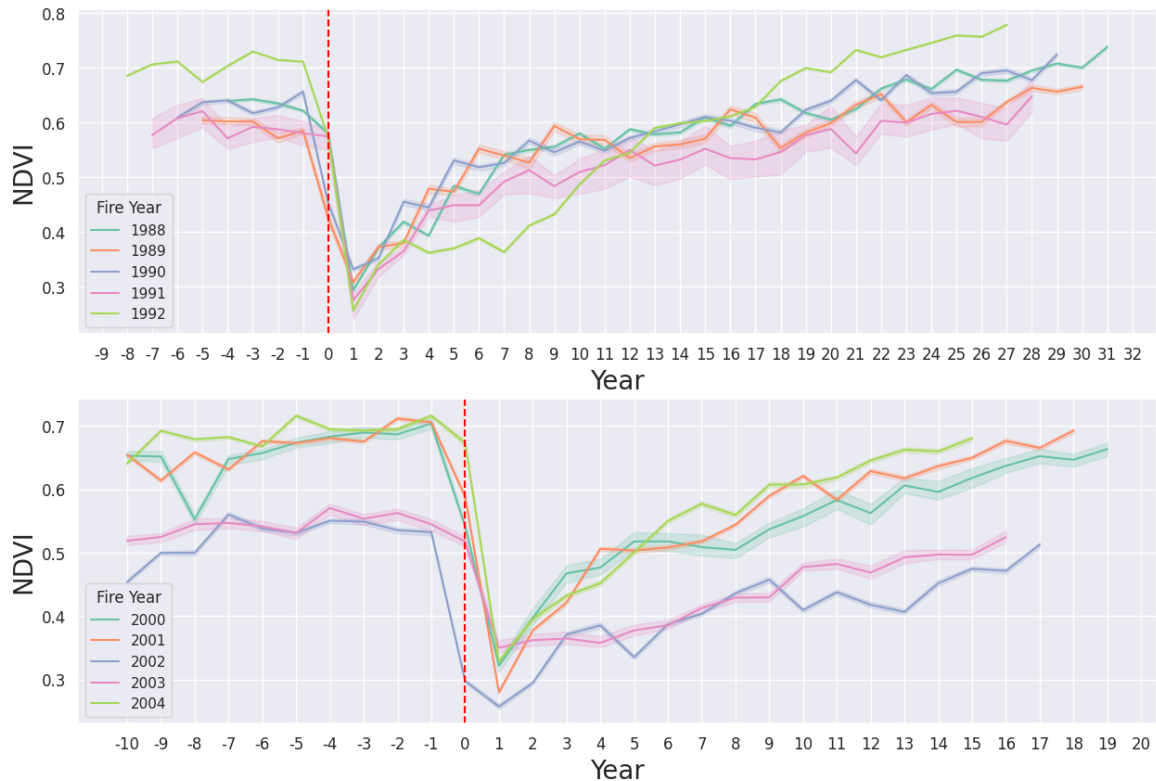


**Fig. A.8** – Time series median NDVI values by fire year. Red, vertical dashed line represents the year of fire, labeled as 0 on the x axis. Values to the left of the line are pre-fire NDVI values, while the values to the right indicate NDVI recovery time series.

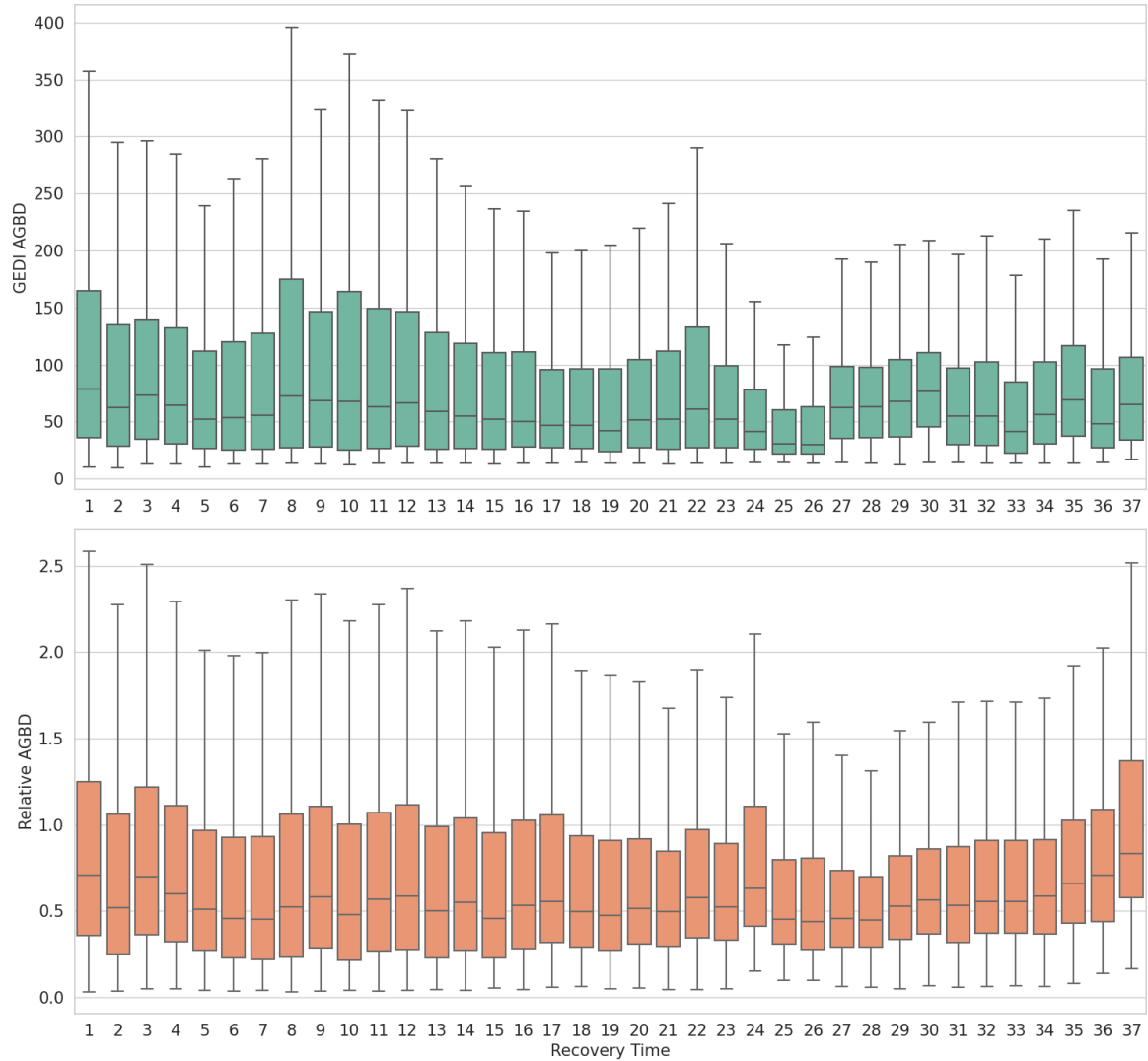


**Fig. A.9 – AGBD recovery reconstructed using space-for-time substitution, for absolute AGBD (top plot) and relative AGBD (bottom plot) values. Data shows a wide spread of values.**

